Automating the IRC Analysis within

Eyringpy

Alan Quintal,[1] Eugenia Dzib,[1] Filiberto Ortíz-Chi,[2] Pablo Jaque,[3] Albeiro Restrepo,[4] and Gabriel Merino.[1,*]

[1]*Departamento de Física Aplicada, Centro de Investigación y de Estudios Avanzados, Unidad Mérida, km 6 Antigua Carretera a Progreso, Apdo. Postal 73, Cordemex, 97310 Mérida, Yucatán, México*

[2]*CONACYT-Universidad Juárez Autónoma de Tabasco, Centro de Investigación de Ciencia y Tecnología Aplicada de Tabasco, Cunduacán 86690, Tabasco, México.*

[3]*Departamento de Química Orgánica y Fisicoquímica, Facultad de Ciencias Químicas y Farmacéuticas, Universidad de Chile, Sergio Livingstone 1007, Independencia, Santiago, Chile.*

[4]*Instituto de Química, Universidad de Antioquia UdeA, Calle 70 No. 51-21, Medellín, Colombia*

gmerino@cinvestav.mx

Abstract

To analyze the evolution of a chemical property along the reaction path, we have to extract all the necessary information from a set of electronic structure computations. However, this process is time-consuming and prone to human error. Here we introduce *IRC-Analysis*, a new extension in *Eyringpy*, to monitor the evolution of chemical properties along the intrinsic reaction coordinate, including complete reaction force analysis. *IRC-Analysis* collects the entire data set for each point on the reaction coordinate, eliminating human error in data capture and allowing the study of several chemical reactions in seconds, regardless of the complexity of the systems. *Eyringpy* has a simple input format, and no programming skills are required. A tracer has been included to visualize the evolution of a given chemical property along the reaction coordinate. Several properties can be analyzed at the same time. This version can analysis the evolution of bond distances and angles, Wiberg bond indices, natural charges, dipole moments, and orbital energies (and related properties).

Introduction

Activation barriers and reaction energies are often not sufficient to understand a reaction mechanism. A better understanding requires a thorough analysis of the evolution of the different geometrical and electronic properties in the course of a chemical reaction. The first step is to divide the reaction into its different elementary reactions. IUPAC[1] defines an elementary reaction as that "*to occur in a single step and to pass through a single transition state*". Once these elementary reactions are established, including the corresponding transition state (TS), the minimum energy pathway (MEP) that connects the TS to the reactant, intermediate or product of interest should be identified. The MEP is usually obtained by calculating the intrinsic reaction coordinate (IRC, or simply ξ).[2-3] IUPAC goes further by defining what is a primitive change in an elementary reaction: "*One of the conceptually simpler molecular changes into which an elementary reaction can be notionally dissected. Such changes include bond rupture, bond formation, internal rotation, change of bond length or bond angle, bond migration, redistribution of charge, etc.*" So, to understand a chemical transformation, we must focus on locating the TS, establishing its MEP, and monitoring its primitive changes.

The information that needs to be extracted and handled from the MEP, via the IRC, to monitor the reaction evolution of primitive changes can be voluminous. If data is handled manually, it can be altered or modified by inherent user errors. With this in mind, we implemented a module in the *Eyringpy* program,[4] called *IRC-Analysis*, to perform this task easily and efficiently, unlike other available options.[5] *Eyringpy* is a modular Python program, launched in 2019, to compute thermochemical properties and rate constants in the

gas phase and in solution. The *IRC-Analysis* module analyses the evolution of various physicochemical properties along the reaction path, including reaction force analysis (RFA). [6] A tracer has also been incorporated to visualize the property changes along the IRC. The properties that can be studied in this version are bond distances, bond angles, Wiberg bond indices, natural charges, orbital energies and dipole moment, but the inclusion of others is straightforward. Another advantage of automating this analysis is that it is carried out in seconds, regardless of the complexity of the system or the number of atoms involved in the reaction.

To show the versatility of our module and its functions, three pericyclic reactions were selected.[7] The first is the degenerate [3,3] Cope rearrangement of 1,5-hexadiene where the RFA is illustrated; the second is the double group transfer (DGT) between ethane and ethylene, which was chosen to exemplify a structural analysis, and finally, the electronic analysis is shown with the electrocyclization of 1,3,5-hexatriene to 1,3-cyclohexadiene.

Input File and Functionalities

Let us describe the *Eyringpy* input file for running the *IRC-Analysis* module. The input file (with the extension *.eif, Figure 1) is divided into four blocks of keywords, placed in any order and case-insensitive.

The first set specifies the reactant(s) (REAC*m*), transition state (TS), and product(s) (PROD*n*) frequency analysis output files, where *m* and *n* are the number of reactants and products involved in the reaction, respectively. The files containing the IRC information must be added using the keyword IRC, and forward and reverse directions can be given in one file or separate files.

In the second set, the user can indicate the properties to be analyzed along the reaction path. These are divided into four categories, depending on the number of atoms involved: none, one, two, and three atoms. For example, since the dipole moment and HOMO-LUMO gap are global properties, no atoms need to be specified. For these cases, the entry "true" in the DIPOLE or HOMOLUMO fields is sufficient. An atom must be defined for the atomic charge analysis (CHARGE keyword), while for bond distances (BONDLENGTH keyword) or bond orders (WIBERG keyword), a pair of atoms must be provided. Finally, for angles (ANGLE keyword), the triad involved must be specified. Properties involving two or three atoms must be separated by a hyphen (-). If the analysis is to be performed on more than one atom, pair, or triad of atoms, these should be separated by a blank space. For the population analysis (bond orders, charges, orbital energies, and dipole moment), the directory path containing the output files of each point along the reaction coordinate must be provided (NBODIR keyword). *IRC-Analysis* will create the input file for each snapshot to perform the NBO calculations by adding the NBOINP keyword, which requires four input values, the memory size, the density functional theory- or wave-function-based method, the basis set, and the population analysis keyword specifications. Examples of structural and electronic working examples are shown in the “Test cases" section.

The third data set is associated with the reaction force analysis. It is activated with the word “true” in the RFORCE keyword. In this version, a spline interpolator (INTERP keyword) is included to compute the reaction force profiles. This interpolator employs a low-degree polynomial, usually three-degree, to connect each pair of points, avoiding Runge’s phenomenon. The main advantage of a spline interpolator is that the resulting curve passes precisely through the input points. Some of the keywords concerning the RFA

and to the interpolation method have default values, keeping the input formats short. Next, the interpolation order (ORDER keyword) must be a positive integer with values between 3 and 5. Its default value is 3, because third-order spline interpolators usually fit well the behavior of energy and reaction force profiles. The next parameter is optional, the number of new points to generate (NPOINTS keywords) with spline interpolation. A thousand points generate smoother energy and reaction force profiles, but this could lead to move the positions of the activated reactants and products. Its default value is zero. The last keyword available in the third data set is DISCRIM. It is used to remove the "noise" from the energy profiles. Some of the points (or all of them) are removed while retaining the values of the original activation and reaction energies. To activate this option, the entry "true" must be indicated in the keyword. An example of reaction force analysis is shown in the "Test cases" section.

The fourth data set is the output options. The XYZ file contains all the structures along the IRC; activating the XYZ keyword with the entry "true" may generate it. The plotter starts by typing the keyword of the property, such as "dipole", "homolumo", "charge", "bondlength", "wiberg", "angle", or "rforce", to be displayed. Multiple properties can be plotted simultaneously by typing the corresponding keywords separated by a blank space.

```
## GAUSSIAN FILES
REACT1    reactant.out
TS        transition-state.out
PROD1     product.out
IRC       irc.out

##PROPERTY ANALYSIS
DIPOLE    true
HOMOLUMO  true
CHARGE    1 2
BONDLEN   1-2 2-3
WIBERG    1-2 2-3
ANGLE     1-2-3
NBODIR    nbo_files

##REACTION FORCE ANALYSIS
RFORCE    true
NPOINTS   0
ORDER     3
DISCRIM   true

##OUTPUT OPTIONS
XYZ       true
PLOT      dipole  charge  wiberg  rforce
```

Figure 1. Example of the use of keywords related to the IRC-Analysis module.

Test Cases

Full geometry optimizations and characterizations for all the test cases were carried out at the M11[8]/6-31+G(d,p)[9-10] level. The nature of the saddle point was characterized at the same level, using harmonic vibrational frequency analysis. The MEP was computed through the IRC in *mass-weighted* internal coordinates,[11-12] using a different step size for each test case. All the computations were carried out using the *Gaussian16* package.[13]

1) Degenerate [3,3] Cope rearrangement of 1,5-hexadiene: Case of the reaction force analysis

The degenerate [3,3] Cope rearrangement of 1,5-hexadiene proceeds synchronously concerted mechanism *via* a chair-like aromatic transition state (Figure 2). The TS structure adopts a C_{2h} symmetry, which implies that the C1-C2 and C4-C5 bond lengths are the same (1.952 Å). The computed relative enthalpy between the TS and 1,5-hexadiene $(\Delta H^{\ddagger})$ is 33.0 kcal mol^{-1}, very similar to the experimental energy barrier of 33.5 kcal mol^{-1}.[14]

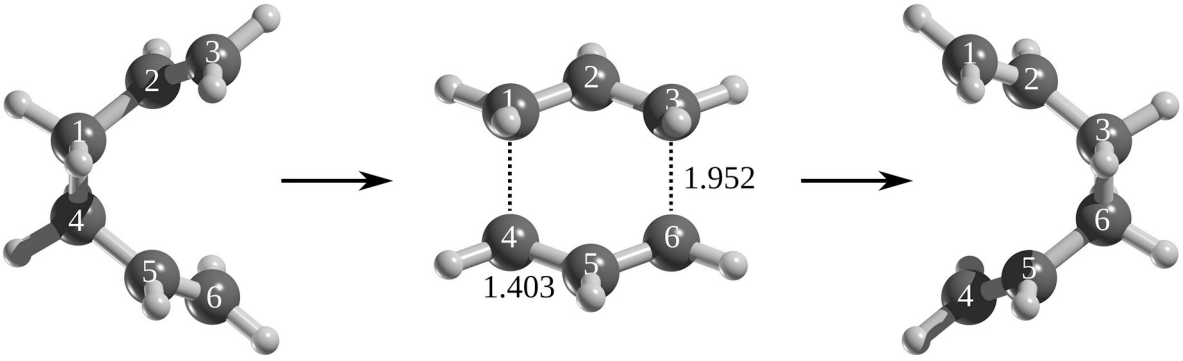

Figure 2. From left to right: reactant, transition state, and product corresponding to the degenerate [3,3] Cope rearrangement of 1,5-hexadiene. Bond lengths are in Angstroms.

In 1999, the group of Toro-Labbé[6] suggested that the analysis of the reaction force (RFA) is a suitable tool for studying reaction mechanisms and identifying the primitive processes in chemical reactions. The reaction force F(ξ), defined as the negative first derivative of the potential energy V(ξ) with respect to the reaction coordinate

$$F(\xi)=\frac{-\partial V(\xi)}{\partial \xi}, \tag{1}$$

has been amply used to understand several chemical reactions such as intra/intermolecular single and double proton transfers,[15-21] conformational changes,[22-23] bond-dissociation and bond-formation,[24-28] S_N2 substitution,[29-30] solvent effects,[31-32] and catalysts.[33-35]

The input file used to process the RFA *via Eyringpy* is shown in Figure 3. This analysis is activated by the entry "true" in the RFORCE keyword. Only the IRC information and the electronic structure files of the reactant, TS and product must be specified.

```
REACT1  1-5-hexadiene.out

PROD1   1-5-hexadiene.out

TS      1-5-hexadiene-ts.out

IRC     irc.out

RFORCE  true
```

Figure 3. *Eyringpy* input file for reaction force analysis of the degenerate [3,3] Cope rearrangement of 1,5-hexadiene.

Figure 4 shows the calculated V(ξ) and F(ξ) profiles of the Cope rearrangement of 1,5-hexadiene using an IRC step size of 0.03 amu$^{1/2}$ bohr. The natural shape of F(ξ) divides the energy paths into four regions, where specific rearrangements take place and produces a partition in the reaction energy. To quantify the amount of work done by each region, F(ξ) must be integrated over a given interval. For example, the forward ($W_{for}^{\ddagger}=W_{I}+W_{II}$) and reverse ($W_{rev}^{\ddagger}=-W_{III}-W_{IV}$) activation barriers and the total reaction work ($W_{rxn}=W_{for}^{\ddagger}-W_{rev}^{\ddagger}$) can be expressed as the sum of these integrals. The reaction work associated with each region of the given reaction and the activation barriers for the forward and reverse paths are summarized in Table 1. The activation energy, $E_{for}^{\ddagger}$=33.9 kcal mol^{-1} ($E_{rev}^{\ddagger}$=33.9 kcal mol^{-1}), of the forward (reverse) process was obtained from the electronic structure files as the energy difference between the TS and the reactant (product). According to the RFA, in elementary reactions, the first step (W_1 or W_4¿ is mainly associated with structural reorganization of the atoms for the forward and reverse processes. In contrast, the second step (W_2 or W_3) is primarily characterized by electronic rearrangement. So, it can be deduced the values in Table 1 that the most significant contributions to the activation works ($W_{for}^{\ddagger}=33.9$ kcal mol^{-1} and $W_{rev}^{\ddagger}=-33.9$ kcal mol^{-1}) are due to structural rearrangements ($W_1=24.0$ kcal mol^{-1} and $W_4=-24.0$ kcal mol^{-1}), which are higher than those associated with the electronic changes ($W_2=9.9$ kcal mol^{-1} and $W_3=-9.9$ kcal mol^{-1}).

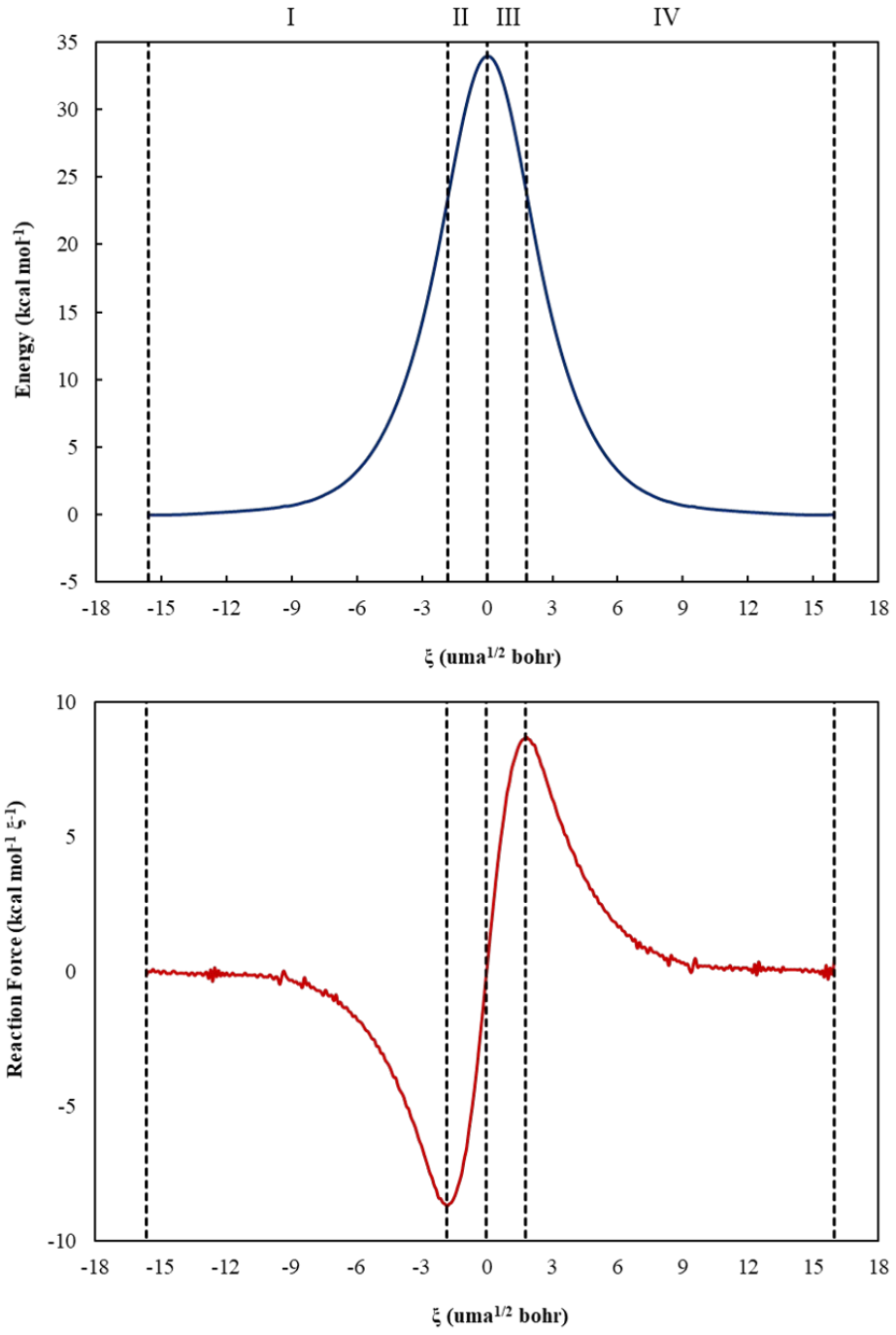

Figure 4. V(ξ), in kcal mol^{-1}, and F(ξ), kcal mol^{-1} ξ^{-1}, profiles of the degenerate [3,3] Cope rearrangement of 1,5-hexadiene calculated with a step size of 0.03 $amu^{1/2}$ bohr. The dashed vertical lines delimit the four regions according to the reaction force analysis.

Table 1. Reaction works associated with the regions of the degenerate [3,3] Cope rearrangement of 1,5-hexadiene computed at the M11/6-31+G(d,p) level for IRC step sizes of 0.03 and 0.05 amu$^{1/2}$ bohr.

	W_1	W_2	W_3	W_4	$W^{\ddagger}_{for}$	$W^{\ddagger}_{rev}$
0.03	24.0	9.9	-9.9	-24.0	33.9	-33.9
0.05	22.7	11.5	-11.5	-22.6	34.2	-34.1
0.05*	22.4	11.5	-11.5	-22.4	33.9	-33.9
$E^{\ddagger}$	-	-	-	-	33.9	-33.9

All values are reported in kcal mol^{-1}. W_n is the amount of work associated with each of the n regions along ξ. $W^{\ddagger}_{for}$ and $W^{\ddagger}_{rev}$ are the activation barriers. Energies calculated with the DISCRIM keyword activated in *Eyringpy*.

One of the main parameters that must be selected in IRC calculations is the size of the IRC steps, in mass-weighted internal coordinates in units of amu$^{1/2}$ bohr. Its typical value is 0.10 amu$^{1/2}$ bohr, but it must be chosen according to the energy profile behavior. Small step sizes are appropriate for curved IRC paths, while large step sizes fit better to flat IRC paths. If the step size is not chosen correctly, the noise in the behavior of the energy profiles could increase and move the activation barriers away from their correct values. The discrimination option in the *IRC-Analysis* module can remove some of the noise on the energy profile, or all, conserving the reaction works and the activation energies ($E^{\ddagger}$). In order to show its function, IRC paths for the degenerate [3,3] Cope rearrangement of 1,5-

hexadiene have been calculated using step sizes of 0.05 amu$^{1/2}$ bohr. 129 snapshots along the reaction path were obtained (see Figure 5). First, the RFA was computed without the DISCRIMN option, obtaining the reaction works ($W_1 = 22.4$, $W_2 = 11.5$, $W_3 = -11.5$ and $W_4 = -22.4$ in kcal mol^{-1}) and activation barriers ($W_{for}^{\ddagger} = 34.2$ and $W_{rev}^{\ddagger} = -34.1$ in kcal mol^{-1}) reported in Table 1. Then, the same calculation was performed but using the DISCIRM option, its input file is shown in Figure 6. Now, the reaction works ($W_1 = 22.4$, $W_2 = 11.5$, $W_3 = -11.5$ and $W_4 = -22.4$ in kcal mol^{-1}) are symmetrical, and the activation barriers ($W_{for}^{\ddagger} = 33.9$ and $W_{rev}^{\ddagger} = -33.9$ in kcal mol^{-1}) are equal to the activation energies ($E^{\ddagger} = 33.9$in kcal mol^{-1}). When the DISCRIM keyword is used, 44 snapshots are removed, giving a smoother energy profile. Figure 5 shows the energy profile with the removed (in black) and no-removed points (in blue). The 129 points are enlisted in Supporting Information.

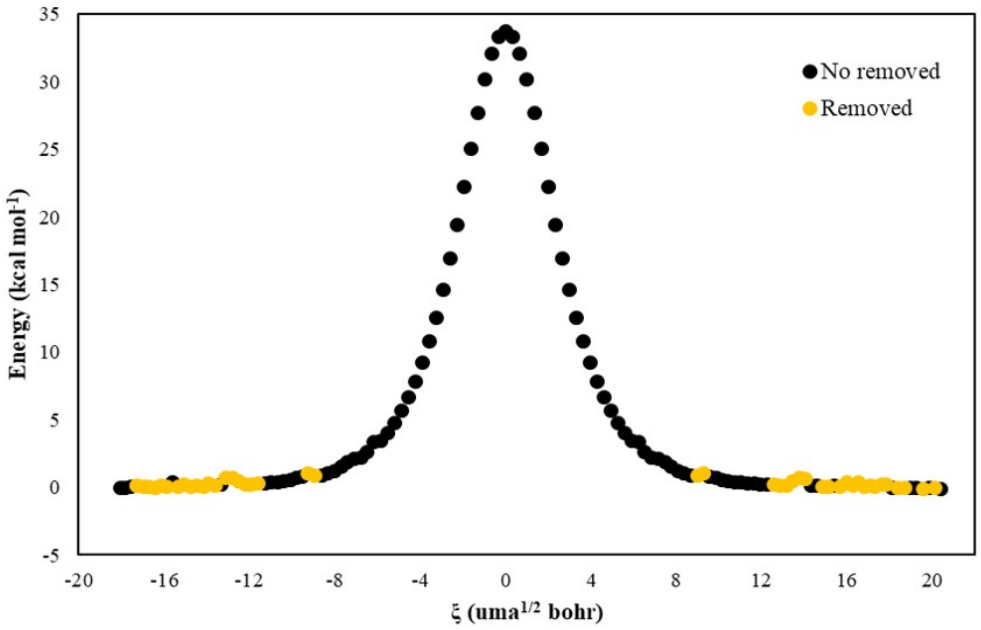

Figure 5. V(ξ) profile of the degenerate [3,3] Cope rearrangement of 1,5-hexadiene calculated with a step size value of 0.05 uma$^{1/2}$bohr, showing the removed (in yellow) and no-removed (in black) points along the IRC using the DISCRIM keyword in the *IRC-Analysis*.

```
REACT1   1-5-hexadiene.out

PROD1    1-5-hexadiene.out

TS       1-5-hexadiene-ts.out

IRC      irc.out

RFORCE   true

DISCRIM  TRUE
```

Figure 6. *Eyringpy* input file for the reaction force analysis of the degenerate [3,3] Cope rearrangement of 1,5-hexadiene using the discrimination option.

2) Double group transfer from ethane to ethylene: Case of the structural analysis

The double group transfer (DGT) reaction is a synchronous transfer of two hydrogen atoms from ethane to ethylene, which occurs through the highly symmetric planar six-membered ring transition structure. The computed activation enthalpy ($\Delta H^{\ddagger}$) was 57.6 kcal mol^{-1}, similar to the value reported at the B3LYP/def2-TZVPP level (58.2 kcal mol^{-1}).[36]

Figure 7 shows the TS structure obtained. The distance between donor/acceptor atoms and hydrogens is 1.369 Å, and the distance between carbon atoms is 1.416 Å, suggesting an aromatic C-C bond length. Similar values were obtained at the B3LYP/def2-TZVPP level (1.372 Å and 1.416 Å, respectively).

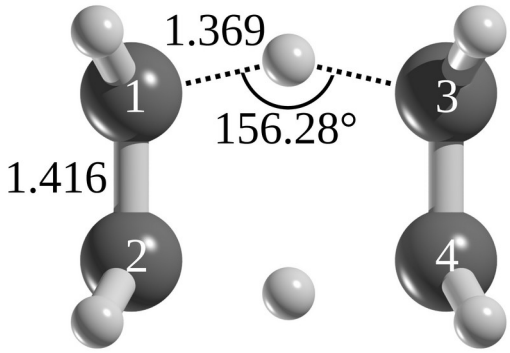

Figure 7. Transition state of the archetypical double group transfer reaction between ethane and ethylene. Bond lengths are in Angstroms.

The corresponding *IRC-Analysis* input file is shown in Figure 8, where numbers 1, 2, 3, and 4 correspond to the carbon atoms, and numbers 5 and 6 to the transferred

hydrogens (see Figure 7). The properties analyzed are bond lengths and angles. Only the IRC information is required to perform this type of analysis, making the input file very short.

```
IRC         for.out   rev.out

BONDLENGTH  1-2 3-4 1-5 3-5 2-6 3-6

ANGLE       1-5-3  2-6-4
```

Figure 8. *Eyringpy* input file of the analysis of the geometric evolution for the double group transfer reaction between ethane and ethylene.

Figure 9a shows the variation of the distance between the donor/acceptor atoms (C3 and C4) with the hydrogens being transferred and the changes in the distances between the donor and acceptor carbon atoms through the IRC. The first part of the reaction is characterized by a rapprochement between the acceptor carbons and the hydrogen atoms. The C3-H and C4-H distances decrease, going from reactants to products, from 2.51 Å to 1.10 Å, while C1-H and C2-H lose their single-bond character. From reactants to products, the C3-C4 bond distance increases from 1.33 to 1.54 Å, whereas the C1-C2 bond decreases from 1.54 to 1.33 Å. This is due to the loss of the double-bond character in the first case (C3-C4) and the transition from single- into double-bond character in the second one (C1-C2).

Figure 9b shows the evolution of the two angles formed by the donor-transferred-acceptor atoms, which have the same behavior in both cases. It is noted that C-H-C angles change by 9°. The hydrogen atoms are located at an intermediate point between the donor

and acceptor atoms in the TS (ξ=0); at this point in the IRC, the C-H-C angles are equal to 156°, and all distances of the atom converge here.

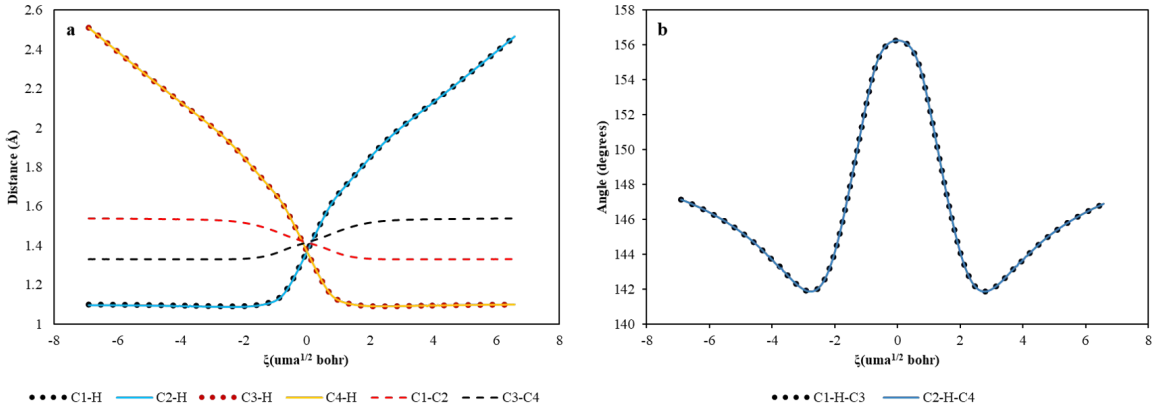

Figure 9. Profiles of **(a)** backbone bond distances (in Ångstroms), and **(b)** angles (in degrees) along the IRC for the double group transfer between ethane and ethylene in degrees.

3) Electrocyclization of *cis*-hexa-1,3,5-triene to 1,3-cyclohexadiene: Case of the electronic analysis

Figure 10 shows the structures related to the electrocyclization of (*Z*)-hexa-1,3,5-triene to 1,3-cyclohexadiene. Note that the lowest structure of the (*E*)-hexa-1,3,5-triene is the C_{2h} as it shows in Table 2, but to carry out electrocyclization requires such a conformational rearrangement, so the reaction takes place at the C_S (*Z*)-hexa-1,3,5-triene to produce C_{2v} 1,3-cyclohexadiene. The typical experimental enthalpy barrier reported for the cyclization of (*Z*)-hexa-1,3,5-triene is 30.2 kcal mol^{-1} in the gas phase.[37] In our case, the relative enthalpy between C_S (*Z*)-hexa-1,3,5-triene and the transition state $(\Delta H^{\ddagger})$ is 30.8 kcal mol^{-1}, computed at the M11 level.

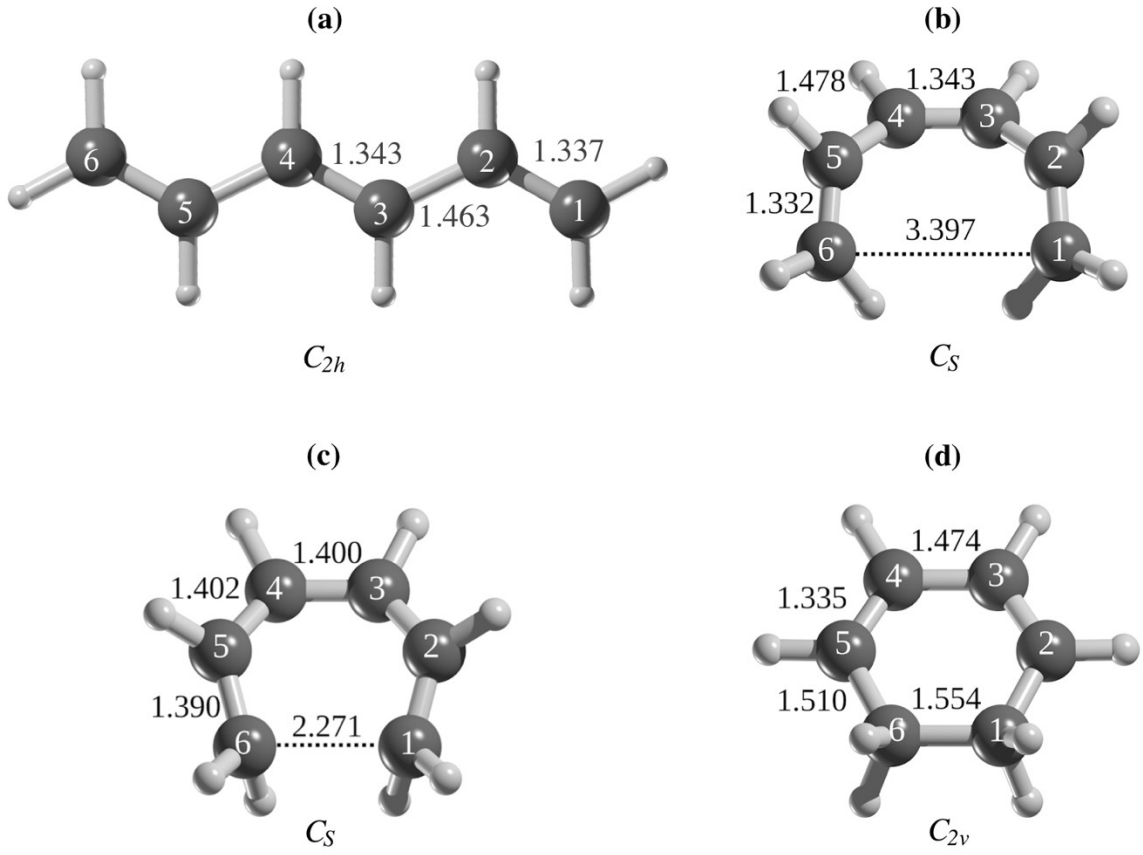

Figure 10. M11/6-31+G(d,p) structures of **(a)** (*E*)-hexa-1,3,5-triene (C_{2h}), **(b)** (*Z*)-hexa-1,3,5-triene (C_S), **(c)** transition state (C_S), and **(d)** 1,3-cyclohexadiene (C_{2v}). Bond lengths are shown in Angstroms.

Table 2. The relative enthalpy free energies ΔH (kcal mol^{-1}) of selected stationary points in the electrocyclization of *cis*-hexa-1,3,5-triene reaction computed at the M11/6-31+G(d,p) level.

	ΔH
(*E*)-hexa-1,3,5-triene (C_{2h})	0.0
(*Z*)-hexa-1,3,5-triene (C_S)	9.5
TS (C_S)	30.9
1,3-cyclohexadiene (C_{2v})	-14.5

All values are reported in kcal mol^{-1}.

The properties considered along the reaction coordinate are the Wiberg bond index, natural charges, dipole moment, and the HOMO-LUMO orbital energies. Before performing this analysis in *Eyringpy*, it is mandatory to have the population analysis calculations of each snapshot along the reaction path. These were estimated using the Natural Bond Orbital (NBO) partition scheme in *Gaussian16* package.[38] The *IRC-Analysis* module was also used to generate the NBO *Gaussian* input files for each structure along the IRC. A total of 78 files were generated. The electronic analysis was then performed using the input file in Figure 11, where numbers 1, 2, 3, 4, 5 and 6 correspond to the carbon atoms (see Figure 10).

```
IRC       for.out   rev.out

NBODIR    nbo_files

WIBERG    1-2 2-3 3-4 4-5 5-6 1-6

CHARGE    1 2 3 4 5 6

DIPOLE    true

HOMOLUMO  true
```

Figure 11. *Eyringpy* input file of the analysis of the electronic evolution for the electrocyclization of (*Z*)-hexa-1,3,5-triene to 1,3-cyclohexadiene

Figure 12a depicts the change of the C-C Wiberg values from two single and three double bonds in (*Z*)-hexa-1,3,5-triene to four single and two double bonds in 1,3-cyclohexadiene. The C1-C2, C3-C4, and C5-C6 bonds change their WBI values from 2.0 to 1.0, and C1-C6 from 0.0 to 1.0, which means that they have acquired a single-bond character. The C2-C3 and C4-C5 bonds change their WBI values from 1.0 to 2.0, forming double bonds in the 1,3-cyclohexadiene. Note that, near the TS, the C1-C6 bond formation has a WBI value of about 0.5, while the remaining bonds' value is approximately 1.5.

Figure 12b shows that the change in natural charge is less pronounced. The carbons forming the C1-C6 bond increase their negative charge by about 0.1 |e|, while their vicinal carbons, C2 and C5, lose 0.06 |e|. The C3 and C4 atoms increase their natural charge only slightly, 0.03 |e|, throughout the reaction. The carbons involved in forming the new bond accept the charge of the other carbon atoms and the hydrogen atoms. In general, the dipole moment increases monotonically throughout the electrocyclization of (*Z*)-hexa-1,3,5-triene

to 1,3-cyclohexadiene, suggesting that the electronic charge changes from a delocalized to a localized feature (Figure 12c). As for the HOMO-LUMO gap, it decreases along the reaction coordinate (Figure 12d), and although the smallest gap is not that of the relaxed structure of 1,3-cyclohexadiene, it can be pointed out that as this reaction is exothermic, the principle of maximum hardness is fulfilled, which establishes that most stable molecular systems tend towards the highest hardness state.[39]

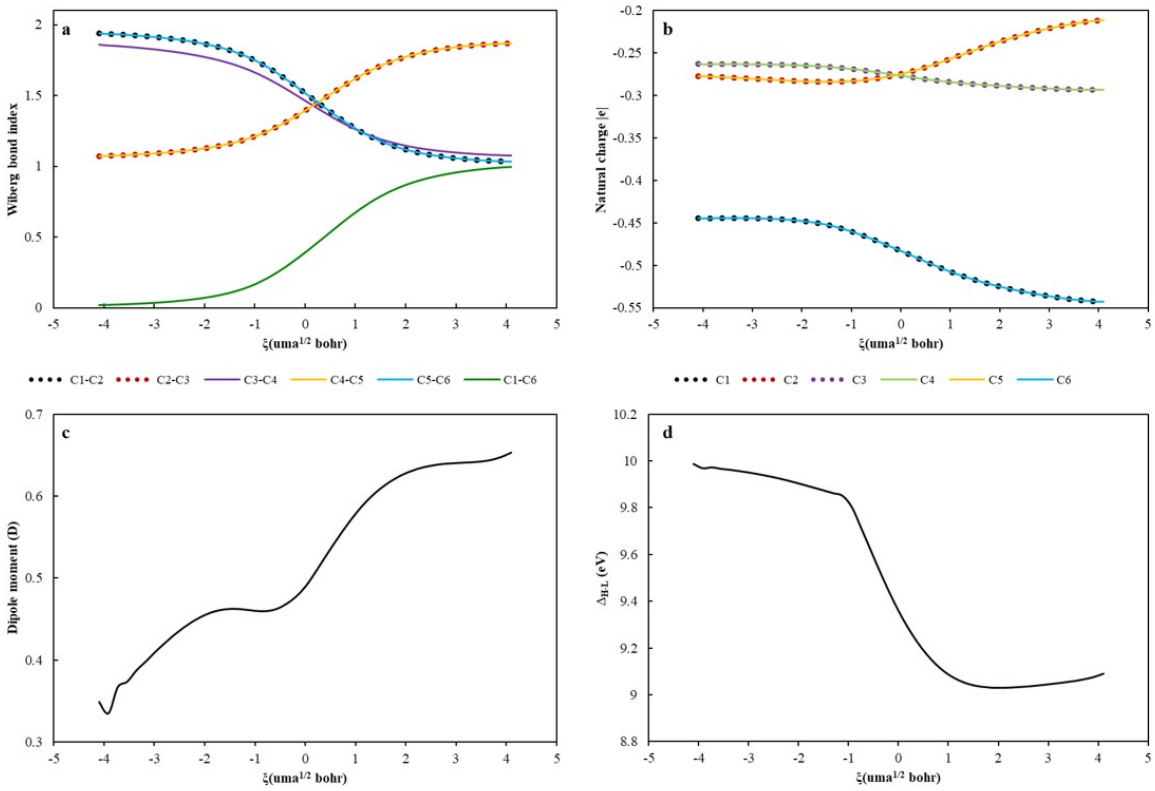

Figure 12. Profiles of **(a)** Wiberg bond indices of all relevant bonds, **(b)** natural charges of all carbon atoms, **(c)** dipole moment (in Debye), and **(d)** HOMO-LUMO gap (in electron-volts) along the IRC for the electrocyclization of (*Z*)-hexa-1,3,5-triene to 1,3-cyclohexadiene.

Summary

We present here *IRC-Analysis*, a new *Eyringpy* module for monitoring the evolution of physicochemical properties along the reaction path, including the reaction force analysis. One of the main advantages of this module is the module data along the reaction coordinate is extracted in a few seconds, eliminating human error in data capture and allowing an easy analysis of several reactions. *IRC-Analysis* includes a plotter for better visualization of the analyzed properties.

The internal structure of the *IRC-Analysis* module is based on subroutines, which facilitates future implementations. This version can analyze atom distances, angles, Wiberg bond indices, natural charges, dipole moments, and HOMO-LUMO gaps. Future versions will include other interpolators, such as Lagrange and Taylor polynomial options, allowing the user to choose the one best suited to a particular energy profile.

The IRC-Analysis module is implemented in *Eyringpy* version 2.0, which can be downloaded free from TheochemMerida's web page: www.theochemmerida.org/eyringpy.

Acknowledgements

AQ and ED thank Conacyt for their PhD fellowships. FOC thanks Conacyt (Grant Al-S-26876) for financial support and Catedras-Conacyt 1024 project. PJ acknowledges to FONDECYT grant with the Project No. 1181914 for the financial support.

REFERENCES

1. Goldbook, I., *R05385. html (accessed May 8, 2014)*.
2. Fukui, K., *J. Phys. Chem.* **1970,** *74* (23), 4161-4163.
3. Fukui, K., *Acc. Chem. Res.* **1981,** *14* (12), 363-368.
4. Dzib, E.; Cabellos, J. L.; Ortíz−Chi, F.; Pan, S.; Galano, A.; Merino, G., *J. Quantum Chem.* **2019,** *119* (2), e25686.
5. Vogt-Geisse, S., *J. Mol. Model.* **2016,** *22* (5), 110.
6. Toro-Labbé, A., *J. Phys. Chem. A* **1999,** *103* (22), 4398-4403.
7. Schleyer, P. v. R.; Wu, J. I.; Cossío, F. P.; Fernández, I., *Chem. Soc. Rev.* **2014,** *43* (14), 4909-4921.
8. Peverati, R.; Truhlar, D. G., *J. Phys. Chem. Lett.* **2011,** *2* (21), 2810-2817.
9. Clark, T.; Chandrasekhar, J.; Spitznagel, G. W.; Schleyer, P. V. R., *J. Comput. Chem.* **1983,** *4* (3), 294-301.
10. Hehre, W. J.; Ditchfield, R.; Pople, J. A., *J. Chem. Phys.* **1972,** *56* (5), 2257-2261.
11. Hratchian, H. P.; Schlegel, H. B., *J. Chem. Phys.* **2004,** *120* (21), 9918-9924.
12. Hratchian, H.; Schlegel, H., *J. Chem. Theory Comput.* **2005,** *1* (1), 61-69.
13. Frisch, M. J.; Trucks, G. W.; Schlegel, H. B.; Scuseria, G. E.; Robb, M. A.; Cheeseman, J. R.; Scalmani, G.; Barone, V.; Petersson, G. A.; Nakatsuji, H.; Li, X.; Caricato, M.; Marenich, A.; Bloino, J.; Janesko, B. G.; Gomperts, R.; Mennucci, B.; Hratchian, H. P.; Ortiz, J. V.; Izmaylov, A. F.; Sonnenberg, J. L.; Williams-Young, D.; Ding, F.; Lipparini, F.; Egidi, F.; Goings, J.; Peng, B.; Petrone, A.; Henderson, T.; Ranasinghe, D.; Zakrzewski, V. G.; Gao, J.; Rega, N.; Zheng, G.; Liang, W.; Hada, M.; Ehara, M.; Toyota, K.; Fukuda, R.; Hasegawa, J.; Ishida, M.; Nakajima, T.; Honda, Y.; Kitao, O.; Nakai, H.; Vreven, T.; Throssell, K.; J. A. Montgomery, J.; Peralta, J. E.; Ogliaro, F.; Bearpark, M.; Heyd, J. J.; Brothers, E.; Kudin, K. N.; Staroverov, V. N.; Keith, T.; Kobayashi, R.; Normand, J.; Raghavachari, K.; Rendell, A.; Burant, J. C.; Iyengar, S. S.; Tomasi, J.; Cossi, M.; Millam, J. M.;

Klene, M.; Adamo, C.; Cammi, R.; Ochterski, J. W.; Martin, R. L.; Morokuma, K.; Farkas, O.; Foresman, J. B.; Fox, D. J., *Gaussian 16* rev. C. 01; Gaussian Inc.: Wallingford CT, 2016.

14. Doering, W. v. E.; Toscano, V.; Beasley, G., *Tetrahedron* **1971,** *27* (22), 5299-5306.
15. Gutierrez-Oliva, S.; Herrera, B.; Toro-Labbe, A.; Chermette, H., *J. Phys. Chem. A* **2005,** *109* (8), 1748-1751.
16. Herrera, B.; Toro-Labbe, A., *J. Phys. Chem. A* **2007,** *111* (26), 5921-5926.
17. Jaque, P.; Toro-Labbé, A., *J. Phys. Chem. A* **2000,** *104* (5), 995-1003.
18. Rincon, E.; Jaque, P.; Toro-Labbe, A., *J. Phys. Chem. A* **2006,** *110* (30), 9478-9485.
19. Toro-Labbé, A.; Gutiérrez-Oliva, S.; Concha, M. C.; Murray, J. S.; Politzer, P., *J. Chem. Phys.* **2004,** *121* (10), 4570-4576.
20. Gomez, S.; Guerra, D.; López, J. G.; Toro-Labbe, A.; Restrepo, A., *J. Phys. Chem. A* **2013,** *117* (9), 1991-1999.
21. Farfán, P.; Echeverri, A.; Diaz, E.; Tapia, J. D.; Gómez, S.; Restrepo, A., *J. Chem. Phys.* **2017,** *147* (4), 044312.
22. Bulat, F.; Toro-Labbé, A., *Chem. Phys. Lett.* **2002,** *354* (5-6), 508-517.
23. Vogt-Geisse, S.; Toro-Labbé, A., *J. Chem. Phys.* **2009,** *130* (24), 244308.
24. Murray, J. S.; Toro-Labbé, A.; Clark, T.; Politzer, P., *J. Mol. Model.* **2009,** *15* (6), 701-706.
25. Politzer, P.; Murray, J. S.; Lane, P.; Toro−Labbé, A., *Int. J. Quantum Chem.* **2007,** *107* (11), 2153-2157.
26. Farfán, P.; Gómez, S.; Restrepo, A., *J. Org. Chem.* **2019,** *84* (22), 14644-14658.
27. Giraldo, C.; Gómez, S.; Weinhold, F.; Restrepo, A., *ChemPhysChem* **2016,** *17* (13), 2022-2034.
28. Gómez, S.; Osorio, E.; Dzib, E.; Islas, R.; Restrepo, A.; Merino, G., *Molecules* **2020,** *25* (2), 284.

29. Giri, S.; Echegaray, E.; Ayers, P. W.; Nuñez, A. S.; Lund, F.; Toro-Labbé, A., *J. Phys. Chem. A* **2012,** *116* (40), 10015-10026.

30. Politzer, P.; Burda, J. V.; Concha, M. C.; Lane, P.; Murray, J. S., *J. Phys. Chem. A* **2006,** *110* (2), 756-761.

31. Burda, J. V.; Toro-Labbe, A.; Gutierrez-Oliva, S.; Murray, J. S.; Politzer, P., *J. Phys. Chem. A* **2007,** *111* (13), 2455-2457.

32. Burda, J. V.; Murray, J. S.; Toro-Labbé, A.; Gutiérrez-Oliva, S.; Politzer, P., *J. Phys. Chem. A* **2009,** *113* (23), 6500-6503.

33. Duarte, F.; Toro-Labbé, A., *Mol. Phys.* **2010,** *108* (10), 1375-1384.

34. Martínez-Araya, J. I.; Quijada, R. l.; Toro-Labbé, A., *J. Phys. Chem. C* **2012,** *116* (40), 21318-21325.

35. Villegas-Escobar, N.; Gutiérrez-Oliva, S.; Toro-Labbé, A., *J. Phys. Chem. C* **2015,** *119* (47), 26598-26604.

36. Fernández, I.; Sierra, M. A.; Cossío, F. P., *J. Org. Chem.* **2007,** *72* (4), 1488-1491.

37. Guner, V.; Khuong, K. S.; Leach, A. G.; Lee, P. S.; Bartberger, M. D.; Houk, K., *J. Phys. Chem. A* **2003,** *107* (51), 11445-11459.

38. Glendening, E.; Reed, A.; Carpenter, J.; Weinhold, F., *Theoretical Chemistry Institute, University of Wisconsin, Madison, WI* **1990**.

39. Pearson, R. G., *J. Chem. Educ.* **1987,** *64* (7), 561.